Characteristics of turbulence-driven plasma flow and origin of experimental empirical scalings of intrinsic rotation

W. X. Wang,[1,a)] T. S. Hahm,[1,b)] S. Ethier,[1] P. H. Diamond,[2] G. Rewoldt,[1] W. M. Tang,[1] and W. W. Lee[1]
[1]*Princeton University, Plasma Physics Laboratory, P. O. Box 451, Princeton, New Jersey 08543*
[2]*University of California, San Diego, La Jolla, California 92093, USA*

(Received 11 January 2011; accepted 17 March 2011; published online 21 April 2011)

Toroidal plasma flow driven by turbulent torque associated with nonlinear residual stress generation is shown to recover the observed key features of intrinsic rotation in experiments. Specifically, the turbulence-driven intrinsic rotation scales close to linearly with plasma gradients and the inverse of the plasma current, qualitatively reproducing empirical scalings obtained from a large experimental data base. The effect of magnetic shear on the symmetry breaking in the parallel wavenumber spectrum is identified. The origin of the current scaling is found to be the enhanced $k_{\|}$ symmetry breaking induced by increased radial variation of the safety factor as the current decreases. The physics origin for the linear dependence of intrinsic rotation on the pressure gradient comes from the fact that both turbulence intensity and the zonal flow shear, which are two key ingredients for driving the residual stress, are increased with the strength of the turbulence drives, which are R/L_{T_e} and R/L_{n_e} for the collisionless trapped electron mode (CTEM). Highlighted results also include robust radial pinches in toroidal flow, heat and particle transport driven by CTEM turbulence, which emerge "in phase," and are shown to play important roles in determining plasma profiles. Also discussed are the experimental tests proposed to validate findings from these gyrokinetic simulations. © *2011 American Institute of Physics*.
[doi:10.1063/1.3575162]

I. INTRODUCTION

Momentum transport and plasma flow generation are complex transport phenomena of great importance in magnetic confinement fusion research. It is generally believed that the prospects for achieving high quality plasma performance in magnetically confined plasmas will be significantly enhanced by optimizing plasma flow characteristics. This can play a critical role in both controlling large-scale (macroscopic) plasma instability and in reducing energy loss due to plasma microturbulence. In current fusion experiments, a large plasma rotation can be driven by neutral beam injection which also provides momentum input while heating the plasma. In large size burning plasmas, however, the use of neutral beams for plasma heating becomes very challenging. On the other hand, it is found that toroidal plasmas can self-organize and develop rotation without an external torque. This intrinsic or spontaneous rotation phenomenon has been widely observed in many fusion devices,[1–5] and is expected to have a major influence on controlling the plasma rotation in the International Thermonuclear Experimental Reactor (ITER). Developing the needed understanding for realistically simulating and modeling the associated dynamics is clearly a high priority area of current research.

Recently, extensive experimental studies have been carried out on this topic. The parametric dependence of the intrinsic rotation has been statistically characterized using a broad range of experimental data bases obtained in multiple machines. Specifically, the increment of central intrinsic rotation is shown to increase with the increment of plasma stored energy and to scale with the inverse of the plasma current (the so-called Rice scaling) for H-mode plasmas without neutral beam heating.[6] Similar empirical scaling is also observed in other devices including JT-60U[7] and large helical device (LHD),[8] where the intrinsic rotation velocity is shown to increase with the ion pressure gradient in core plasmas with an internal transport barrier (ITB). There is no doubt that these results are important for making a qualitative projection of plasma rotation in ITER. A more fundamental, critical issue is to understand the underlying physical origins of the experimental empirical scalings. This is the major focus of this study.

Out of various possibilities of physical dynamics which may play roles in determining toroidal rotation, the strong coupling between toroidal momentum and energy transport generally observed in fusion experiments[9–11] suggests that microturbulence is a key player. For turbulence-driven toroidal momentum flux, a generic structure can be expressed as follows:

$$\Gamma_\phi \propto -\chi_\phi \frac{\partial U_\phi}{\partial r} + V_p U_\phi + \Pi^{rs}_{r,\phi},$$

where U_ϕ is the toroidal rotation velocity. In addition to diffusion (first term with χ_ϕ the momentum diffusivity), there are two nondiffusive components, momentum pinch (second term with V_p the pinch velocity) and residual stress (third term).

[a)]Author to whom correspondence should be addressed. Electronic mail: wwang@pppl.gov.
[b)]Present address: Seoul National University, Department of Nuclear Engineering, Seoul, Republic of Korea.

The three components in the momentum flux are highly distinct not only formally but also physically. Besides their different physical origins under turbulence circumstances, they have qualitatively distinct effects on the toroidal flow formation. Note that all three components have been observed in tokamak experiments.

The residual stress $\Pi^{rs}_{r,\phi}$ is defined as a specific part of the Reynolds stress with no direct dependence on either the rotation velocity or its gradient. Apparently, a fundamentally distinct effect of residual stress is that it can generate local toroidal momentum in a rotation-free plasma, which, incorporating proper boundary effects at (flux) surfaces enclosing the plasma, offers an ideal mechanism to drive mesoscale intrinsic rotation. In a broad physical context, this is a type of wave-driven flow phenomenon which operates via wave–particle resonant interaction.[12] In experiments, the existence of intrinsic torque is confirmed by the fact that a net neutral-beam-induced external torque is required to counter-balance intrinsic torque in order to hold the plasma stationary without rotating.[13]

Systematic global gyrokinetic simulations using experimentally relevant parameters have revealed an important nonlinear flow generation process due to the residual stress produced by electrostatic turbulence of ion temperature gradient (ITG) modes and trapped electron modes (TEM).[14,15] Both fluctuation intensity and intensity gradient were identified to drive residual stress. A generic, key ingredient for turbulence-driven residual stress is the presence of asymmetry in the parallel wavenumber spectrum,[12] which can be obtained via various mechanisms.[14,16–21] In the idealized case, for most drift wave instabilities, both signs of $k_\parallel$ are equally excited, resulting in a reflection symmetry in the $k_\parallel$ spectrum. Perfect local $k_\parallel$ symmetry means perfectly balanced population density between co- and counter-propagating acoustic waves along the torus, and thus a vanishing net local momentum torque. Therefore, a critical, generic piece of physics behind the residual stress spinning up the plasma is the breaking of the $k_\parallel \rightarrow -k_\parallel$ symmetry and the generation of a nonvanishing averaged $\langle k_\parallel \rangle$. Concerning the origin of the symmetry breaking, turbulence self-generated low frequency zonal flow shear has been found to be a key, general mechanism in various turbulence regimes. Simulations and theory also suggest other mechanisms beyond $\mathbf{E} \times \mathbf{B}$ shear effects.[15,19,21–26]

In this work, the characteristic dependence of the turbulence-driven intrinsic rotation on plasma parameters is investigated using the global Gyrokinetic Tokamak Simulation (GTS) code[27] with focus on understanding the underlying physics associated with the experimental empirical scalings of intrinsic rotation. The GTS code is a global, δf particle-in-cell code based on a generalized gyrokinetic simulation model and the use of realistic magnetic configurations. It incorporates the comprehensive influence of noncircular cross section, realistic plasma profiles, plasma rotation, neoclassical (equilibrium) electric field, Coulomb collisions, and other features.

Our focus is on the electron transport dominated regimes that are highly significant for ITER, but which are difficult to access in current experiments. To simulate electron turbulence and ion turbulence with nonadiabatic electron physics, fully kinetic electron physics is included in the GTS code.[15] One highlighted feature, distinct from many other gyrokinetic simulations, is that both trapped and untrapped electrons are included in the nonadiabatic response.

The remainder of this paper is organized as follows. In Sec. II, characteristics of turbulence nonlinearly-driven plasma flows are investigated. The primary purpose is to attempt to shed light on the physics origin of empirical scalings of intrinsic rotation. In Sec. III, mesoscale phenomena in collisionless trapped electron mode (CTEM) turbulence, including flows, and particle and heat pinches, are discussed. A summary and discussion are given in Sec. IV.

II. CHARACTERISTIC DEPENDENCE OF TURBULENCE DRIVEN TOROIDAL ROTATION

The turbulence-nonlinearly-driven residual stress, acting as an intrinsic torque, spins up toroidal rotation effectively. In our previous study, ITG turbulence-driven "intrinsic" torque was shown to increase close to linearly with ion pressure gradient,[15] in qualitative agreement with experimental observations in various devices[6–8] including more recent I-mode plasmas in C-MOD.[28] More recently, a theoretical model of a plasma "engine" was used to capture a similar scaling behavior for ITG-driven flow with adiabatic electrons.[29] For certain plasma parameters of fusion experiments, collisionless TEM turbulence can be a major source to drive multiple-channel transport, including toroidal momentum transport. However, the momentum transport and flow generation phenomena have not been well explored experimentally in the electron transport dominated regimes. Quantifying the characteristic dependence of turbulence generated toroidal flow in the electron turbulence regimes is particularly important for ITER experiments in which the electron channel is expected to dominate plasma transport.

The characteristic dependence of intrinsic torque driven by CTEM turbulence is numerically investigated in this section. The GTS simulations are carried out over a wide range of experimentally relevant plasma parameters, which cover various regimes with respect to different sources of free energy for driving CTEM turbulence.

A. Dependence of turbulent torque on electron profile gradients

First, we explore the relationship between turbulence-driven residual stress and associated intrinsic torque and electron profile gradients. For this parametric scan study, radial profiles of electron density/temperature gradient used in simulations are specified according to the expression: $R_0/L_{n_e,T_e} = -\kappa \exp\left[-(\rho - \rho_c/0.28)^6\right]$, along with a fixed density/temperature at the center $\rho_c = 0.5$ (in terms of normalized minor radius). This gives a fairly uniform CTEM drive in a region centered at ρ_c and near zero gradient elsewhere. The simulation scan is performed by varying the κ value. Note that these gyrokinetic simulations are performed on the turbulence time scale which is much shorter than the transport time scale for significant evolution of plasma profiles. Thus, the effect of profile evolution during a simulation

is small. The simulation domain is from $\rho = 0.1$ to $\rho = 0.9$. As a general feature of global gyrokinetic simulations, one must specify boundary conditions in the radial direction, unlike local flux-tube simulations which normally use periodic boundary conditions. In all simulations in this paper, absorbing boundary conditions are used by applying a damping effect in very narrow boundary layers, typically, at $\rho > 0.8$ and $\rho < 0.2$, which work to remove fluctuations coming from the unstable core region that reach the boundaries. This may correspond to certain realistic situations, for which the influence from the outside of the simulated plasma region is negligible. For all simulations presented in this paper, plasmas are initially rotation-free and momentum-source-free, which allows us to concentrate on the residual stress and associated intrinsic torque. An equilibrium $\mathbf{E} \times \mathbf{B}$ shear is also included via the radial force balance relation, which, however, is seen to be a minor player with respect to CTEM self-generated zonal flows. The numerical magneto-hydrodynamic (MHD) equilibrium used in this study corresponds to a real DIII-D discharge. Other major parameters used include: $R_0/L_{T_i} = 2.4$, $T_e/T_i = 1.2$ at the center ($\rho = 0.5$), and perpendicular grid size $\Delta_\perp \sim 0.5\rho_s$ (locally) which allows for sufficient spatial resolution for CTEM turbulence with specified parameters. All simulations in this paper use 100 particle/cell × species. Convergence studies have shown that the so-called noise-induced transport in our simulations is negligible compared to the turbulence-driven transport.[15]

Before presenting our major results concerning the primary issue of this paper, it is necessary to examine how a net ion toroidal momentum (rotation) at the mesoscale is produced. Typical results for CTEM turbulence are illustrated in Fig. 1. At an early phase, radially local toroidal momentum (rotation) is produced in either one of both co- and counter-current directions in the central core turbulence region due to the local turbulent torque associated with nonlinear residual stress generation. This is illustrated by the black curve in the left panel of Fig. 1, which shows a radial profile of toroidal momentum density p_ϕ at $t = 100$. The gyrokinetic description of tokamak plasmas is shown to conserve toroidal momentum.[30,31] It is remarked that the total (volume-integrated) toroidal momentum $P_\phi \equiv \int p_\phi d^3r$ is close to zero, and indeed is approximately conserved in the simulation until a well saturated nonlinear phase ($t < 110$), as seen in the right panel of Fig. 1. A net toroidal momentum starts to develop in the co-current direction after this point when turbulence fluctuations reach the boundaries of the simulated plasma and begin to be affected by them. Note that the total momentum increases at a nearly constant rate. Besides the fundamentally key role of nonlinear residual stress, this complicated process may involve several important effects. First, the total momentum density inside the plasma consists of contributions from resonant particles and waves, and momentum exchange between them occurs through resonant wave–particle interaction. The radial transport behavior between wave-momentum and resonant particle-momentum is different because of highly distinct features of the associated momentum fluxes (i.e., residual stress) between them.[12] As a consequence, wave-momentum and particle-momentum are dissipated at the boundaries at different rates (presumably, mostly wave-momentum is absorbed at the boundaries), leaving a net nonvanishing momentum inside the plasma. Particle flux driven by CTEM fluctuations also plays a role. Particle flux can influence the rotation profile formation by carrying a convective flux of toroidal momentum once local toroidal momentum is generated due to the residual stress. Finally, toroidal momentum can be exchanged between ions and electrons. However, this effect should be less significant because of the small e-i mass ratio.

Instead of calculating the local torque $\nabla \cdot \Pi^{rs}_{r,\phi}$, we examine the rate of toroidal momentum generation, dP_ϕ/dt, associated with the residual stress. Apparently, the quantity dP_ϕ/dt is a measure of the volume-integrated (or spatially averaged) torque driven by turbulence, which has better correspondence to the intrinsic torque inferred from experiments or measured central intrinsic rotation. The simulation results for total intrinsic torque dP_ϕ/dt driven by CTEM turbulence versus the electron pressure gradient ∇p_e are summarized in Fig. 2, in which three curves correspond to three cases of free energy for driving CTEM. The dominant free energy sources are ∇n (black), ∇T_e (green) and a combination of both (red), respectively. For all three cases, the turbulence-driven torque associated with nonlinearly generated residual stress is found to increase close to linearly with the electron pressure gradient. In other words, a larger central intrinsic rotation is expected to be produced in a plasma with a higher electron pressure gradient. The dominant underlying physics governing this scaling is rather straightforward, namely, both the turbulence intensity and the zonal flow shear, which are the two key ingredients for driving residual

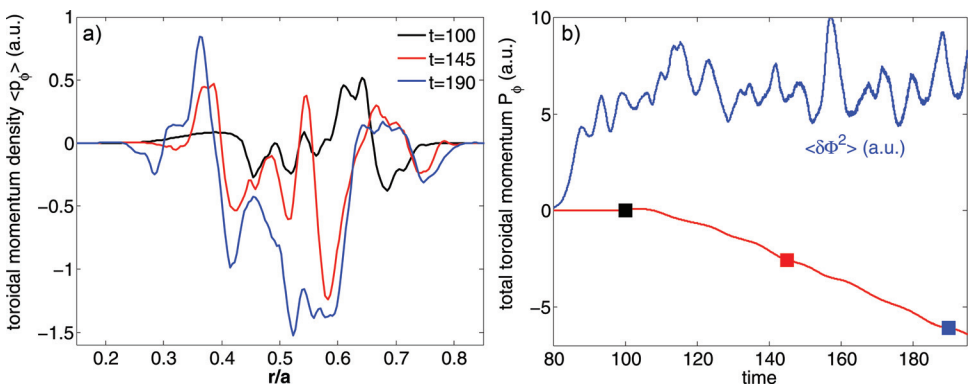

FIG. 1. (Color online) Radial profile of toroidal momentum density at three different times (left), and time history of volume-integrated toroidal momentum (with three marks corresponding to the three curves in the left panel), and turbulence intensity at a central location $\rho = 0.5$ (right).

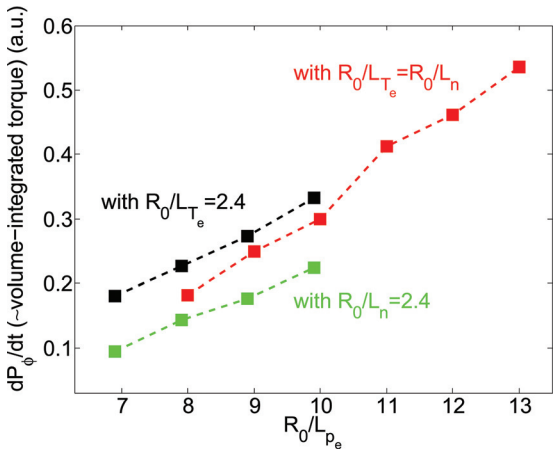

FIG. 2. (Color online) CTEM-driven total intrinsic torque (spatially averaged) vs electron pressure gradient R_0/L_{p_e}.

stress, are increased with the strength of the CTEM drive R_0/L_{p_e}. Moreover, the observation of the black curve being above the green and red curves indicates that the free energy in the density gradient is more efficient than that in the temperature gradient in driving intrinsic rotation via CTEM turbulence. One robust feature of CTEM-driven intrinsic rotation is also highly remarkable, namely, the intrinsic rotation is generated mostly in the co-current direction, which appears to be consistent with the trend of experimental observations in H-mode plasmas.[6] These results predicted from the gyrokinetic simulations suggest a strong connection between intrinsic rotation and electron parameters, which may have important implications, particularly for ITER experiments. It will be highly interesting to test this prediction in experiments. As a good opportunity for validation study, particularly, National Spherical Torus Experiment (NSTX) experiments can be used as a unique platform to test the predicted characteristic dependence of intrinsic rotation on electron parameters in electron transport dominated regimes.

B. Current scaling of turbulence-driven intrinsic torque

Now we turn to exploring the dependence of turbulence-driven residual stress and intrinsic rotation on the plasma current I_p. Again, this simulation study is carried out for CTEM turbulence. The primary purpose is to attempt to shed light on the physics origin of the current scaling which was obtained in multiple devices.[6] For this simulation study we adopt a similar methodology to that used in experiments for various investigations of current scans. A set of simulation experiments is carried out by holding the vacuum (external) magnetic field and plasma pressure profile fixed, while varying the plasma current. Specifically, this is accomplished by generating a series of shaped, numerical equilibria with $I_p = 0.75$, 1.0, 1.5, and 2.0 MA, using an MHD code named ESC.[32]

The plasma gradients used for this study are: $R_0/L_{T_e} = R_0/L_n = 6$ and $R_0/L_{T_i} = 2.4$ with $T_e/T_i = 1.2$. Simulation results presented in the top-left panel of Fig. 3 show that the rate of toroidal momentum generation by CTEM turbulence (i.e., total turbulent torque) increases close to linearly with the inverse of the plasma current. This result indeed reproduces the same trend as that of the Rice scaling. CTEM turbulence is well known to drive plasma transport in multiple channels. It is highly interesting to compare this result of toroidal momentum transport with those of turbulence-driven heat and particle transport. The results of simulated particle and electron heat fluxes are presented in the upper-middle panels of Fig. 3, which show that CTEM-driven heat/particle fluxes are nearly at the same level for the four cases. In other words, turbulent particle and heat transport are roughly independent of the plasma current in this scan, in contrast to the turbulent torque.

With respect to the torque versus ∇T, ∇n, and ∇p scaling in ITG and CTEM turbulence, the underlying physics governing the current scaling is less transparent. Both turbulence intensities and intensity gradients are shown to drive the residual stress. First, we examine the turbulence intensity levels of four cases. As is also shown in the top panel of Fig. 3, the volume-integrated turbulence intensities in the steady state are actually at the same level for the four cases, roughly independent of the current. This is consistent with the results of the simulated heat and particle fluxes whose magnitudes, in general, are believed to be more primarily coupled with fluctuation intensity than other turbulence related quantities, and thus are insensitive to variation in the plasma current also. At the same time, the turbulence intensity gradient, which can also contribute to driving residual stress with an asymmetric fluctuation spectrum in $k_\parallel$ due to turbulence wave radiation induced wave-momentum diffusion,[33] also does not show significant current dependence that can account for the torque vs I_p scaling observed in our simulations. Hence, these results imply that the underlying physics for the current scaling has to do with the symmetry breaking dynamics and the associated mechanisms. This critical point is further directly elucidated by examining the amplitude of the spectrum-averaged parallel wavenumber, defined as

$$\langle k_\parallel \rangle (r) \equiv \frac{1}{qR_0} \frac{\sum (n/|n|)(nq-m)\delta\Phi_{mn}^2}{\sum \delta\Phi_{mn}^2},$$

which serves as a quantitative measurement for how strongly the $k_\parallel$ symmetry is broken.[14] Here $\delta\Phi_{mn}$ is a mode amplitude, with m and n the poloidal and toroidal mode numbers, respectively. The results for the two cases with $I_p = 1.5$ MA and $I_p = 0.75$ MA are presented in the lower-middle-panels of Fig. 3, which show that the overall amplitude of $\langle k_\parallel \rangle$ in the primary region of CTEM fluctuations is significantly increased (by a factor of $\gtrsim 2$ as indicated by the color bars) as the plasma current is halved. Consistent with the enhanced $k_\parallel$ symmetry breaking, the CTEM generated intrinsic torque is roughly doubled from the $I_p = 1.5$ MA case to the 0.75 MA case.

Now, the key issue turns out to be the understanding of what makes the difference in the symmetry breaking when varying the plasma current. As we found previously, the turbulence self-generated zonal flow shear provides a generic mechanism for the symmetry breaking. The $\mathbf{E} \times \mathbf{B}$ shearing rates of zonal flows corresponding to the above two cases

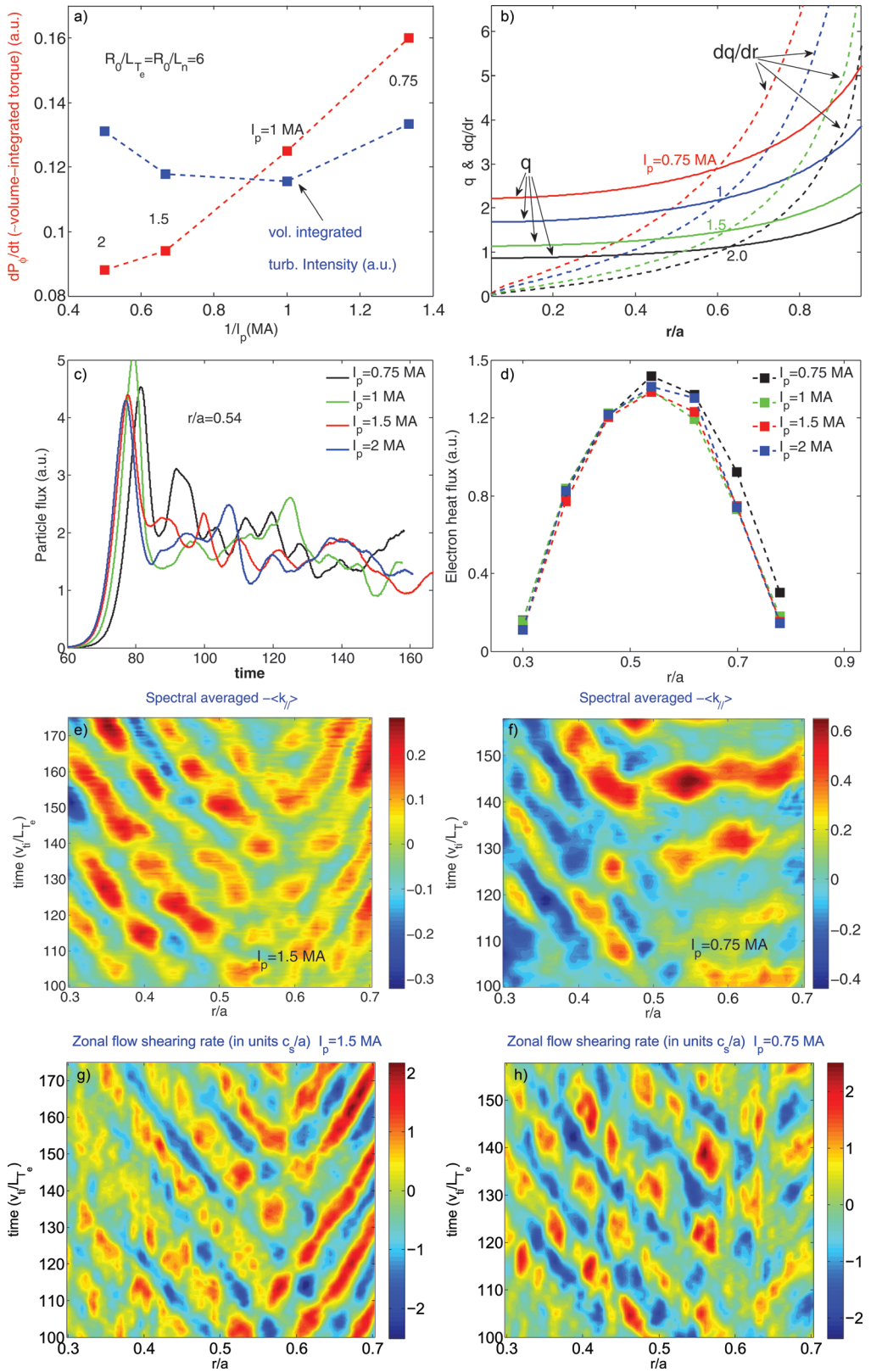

FIG. 3. (Color online) CTEM-driven total intrinsic torque and volume-integrated turbulence intensity at steady state vs plasma current I_p (top-left), and radial profiles of q and dq/dr of the four equilibria used in this scan (top-right); CTEM-driven particle fluxes vs time at a central radial location where dominant CTEM fluctuations are present (upper-middle-left), and steady state electron heat fluxes vs $\rho = r/a$ (upper-middle-right); spatio-temporal evolution of spectrum-averaged parallel wavenumber—$\langle k_\parallel \rangle$ for two cases with $I_p = 1.5$ MA (lower-middle-left) and $I_p = 0.75$ MA (lower-middle-right); and spatio-temporal evolution of zonal flow shearing rate for $I_p = 1.5$ MA (bottom-left) and $I_p = 0.75$ MA (bottom-right).

with different I_p values are presented in the bottom panels of Fig. 3, which, however, are found to be very comparable. The color bars clearly show that the zonal flow shearing rates are on the same level. This indicates that the difference generated in the symmetry breaking level is not associated with the zonal flow shear. While zonal flow shear is a common element providing symmetry breaking in $k_\parallel$, our previous simulations also indicated the existence of other mechanisms beyond $\mathbf{E} \times \mathbf{B}$ shear. These include the radial variation of the safety factor, to be discussed below.

Note that, on the other hand, the corresponding q profile is remarkably boosted in the four equilibria as the plasma current is decreased from 2 to 0.75 MA; so is its radial variation, dq/dr (the top-right panel of Fig. 3). Also note that the parameter ρ_* ($\equiv \rho_i/a$) for the four cases is roughly the same, i.e., $\rho_* \sim 1/170$, which is in the Doublet III-D (DIII-D) range. This observation is highly suggestive that the current scaling of intrinsic torque and rotation may have connections with the change in the value of q and/or its radial variation.

To identify the effects of the safety factor and the radial variation of it, separately, further computational experiments are performed. First, we examine the effect of the q value. To this end, three MHD equilibria are created, which hold the profile of dq/dr (and plasma pressure) fixed while boosting the q profile, as shown in the upper-right panel of Fig. 4. For this scan, the CTEM-driven intrinsic torque is found to decrease with the increase in the q value, as illustrated in the upper-left panel of Fig. 4. The spectrum-averaged parallel wavenumber displayed in the lower panels of Fig. 4 for the two cases with averaged $\bar{q} = 1.33$ and $\bar{q} = 2.33$ show that the overall amplitude of $\langle k_\parallel \rangle$ in the primary region of CTEM fluctuations is on the same level, as indicated by the color bars. This result shows that the effect of change in the q value on the $k_\parallel$ symmetry breaking is weak. On the other hand, the dependence of the volume-integrated turbulence intensity on the q value plotted in the upper-left panel of Fig. 4 indicates that this turbulence intensity dependence appears to be a major cause for the observed intrinsic torque vs q dependence. The key point of this interesting result, however, is that the dependence of the torque on the q value shows the opposite trend to the current scaling obtained in Fig. 3. Therefore, the current scaling cannot be established

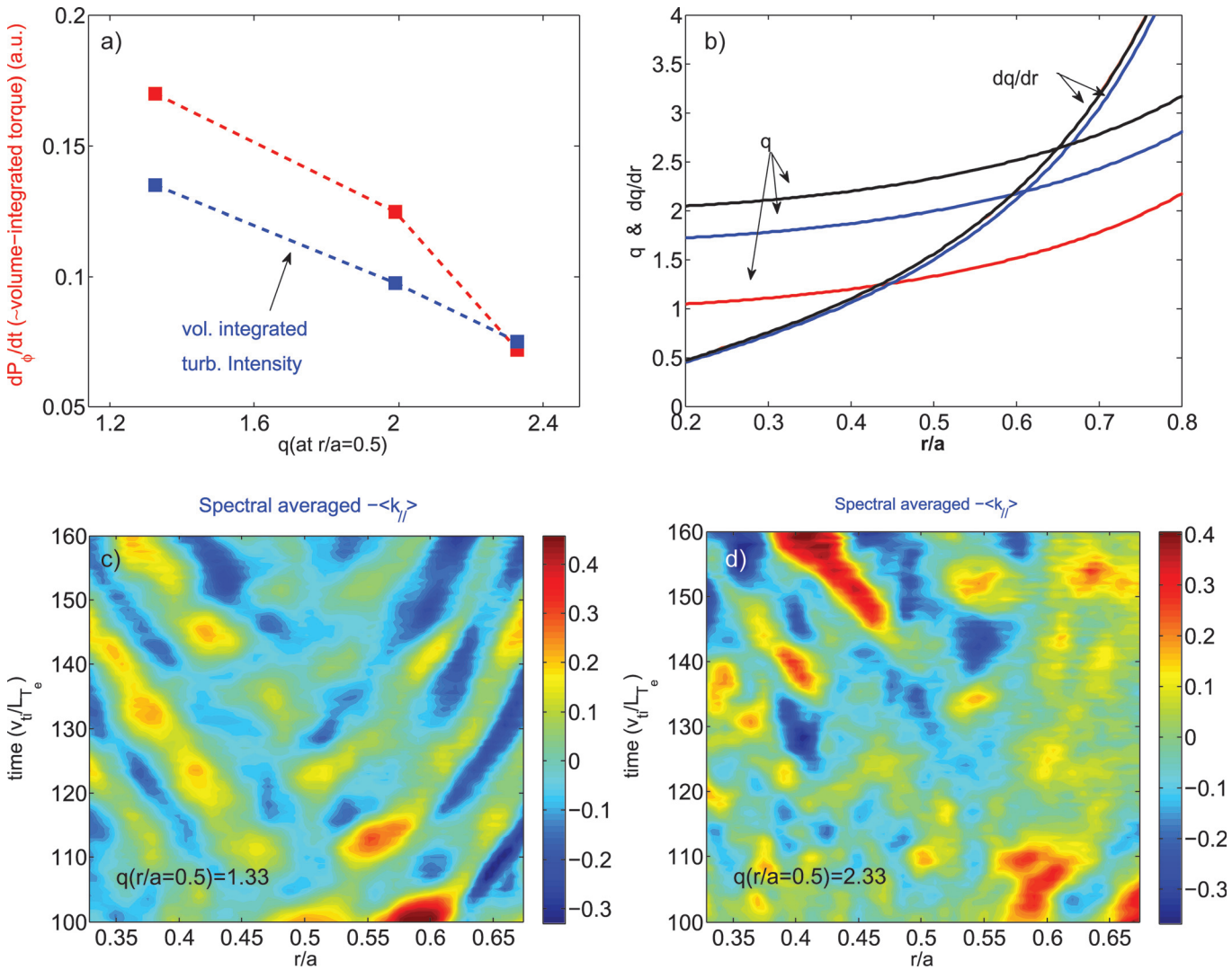

FIG. 4. (Color online) CTEM-driven total intrinsic torque vs q value averaged over the central core region (upper-left) and the corresponding radial profiles of q and dq/dr for the three equilibria used for these simulations (upper-right), and spatio-temporal evolution of spectrum-averaged $\langle k_\parallel \rangle$ for two cases with $\bar{q} = 1.33$ (lower-left) and $\bar{q} = 2.33$ (lower-right).

through the effect of the q value on the nonlinear residual stress generation.

Now we turn to exploring the effects of the radial variation of q on the turbulence-driven torque. To this end, three MHD equilibria are created, which hold the radially averaged q value nearly fixed in the central core region where CTEM turbulence is generated, but allow minor variation in the q profile in order to create significant variation in dq/dr, as illustrated in the middle panels of Fig. 5. At the same time, the plasma pressure is held fixed. Note that a normal

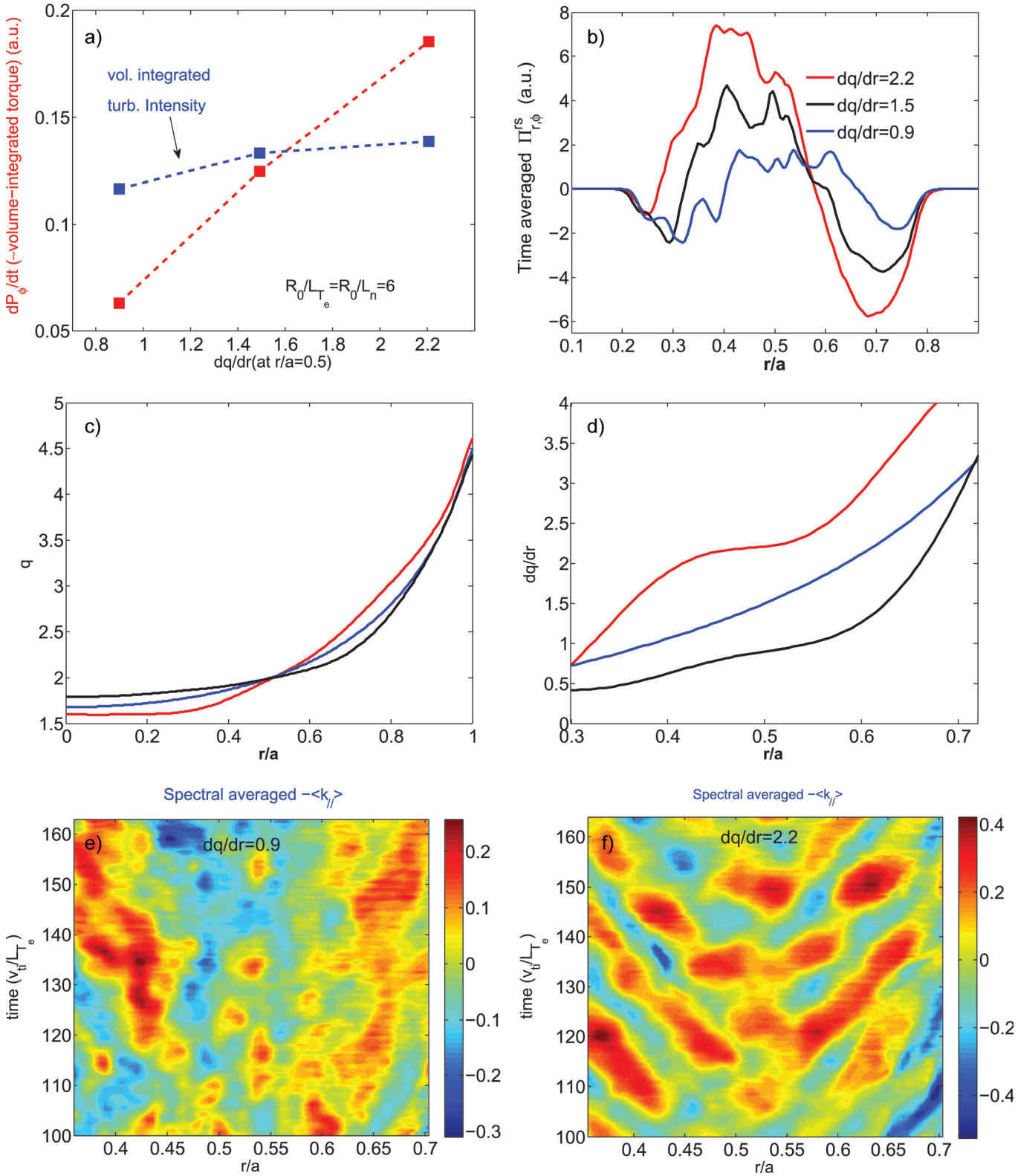

FIG. 5. (Color online) CTEM-driven total intrinsic torque vs the radial variation of q averaged over the central core region (top-left), and radial profiles of mean residual stress at steady state (top-right); corresponding radial profiles of q (middle-left) and dq/dr (middle-right) for the three equilibria used for these simulations; spatio-temporal evolution of spectrum-averaged $\langle k_\parallel \rangle$ for two cases with averaged $dq/dr = 0.9$ (bottom-left) and $dq/dr = 2.2$ (bottom-right).

(positive) magnetic shear is present in all equilibria used in this paper. The primary result of this simulation scan is presented in the top-left panel of Fig. 5, which shows that the volume-integrated turbulent torque (i.e., the momentum generation rate) increases nearly linearly with dq/dr. This scaling trend of the turbulent torque is consistently supported by the results of the underlying residual stress generation. The radial profiles of the residual stress (time averaged over steady state) for the three cases with different dq/dr are presented in the top-right panel of Fig. 5. The residual stress $\Pi^{rs}_{r,\phi}$ is calculated according to the following kinetic definition for the toroidal momentum flux:

$$\Gamma_\phi \equiv \langle \int d^3 v m_i R v_\phi \mathbf{v}_E \cdot \nabla\rho/|\nabla\rho| \delta f_i \rangle,$$

where m_i, v_ϕ, and $\mathbf{v}_E \cdot \nabla\rho/|\nabla\rho|$ are ion mass, toroidal velocity, and radial $\mathbf{E}\times\mathbf{B}$ drift velocity, respectively, δf_i is the perturbed ion distribution function, and $\langle\ \rangle$ denotes flux surface average. Because of the zero initial toroidal rotation used in these simulations, the calculated momentum flux is, by definition, essentially residual stress. The result in Fig. 5 shows that the residual stress generation is enhanced as dq/dr increases. One may notice that the mean residual stress at steady state changes direction, typically from outward in the inner core region to inward in the outer core region. This feature of turbulent residual stress is highly robust in our CTEM simulations. What determines the sign of the residual stress, particularly its relation with plasma parameters, remains to be understood. At the same time, the volume-integrated fluctuation intensity exhibits a much weaker dependence on dq/dr (top-left panel of Fig. 5), which indicates that the observed intrinsic torque vs dq/dr scaling mostly results from the effect of the $k_\parallel$ symmetry breaking physics. Indeed, this is directly clarified by the results of the spectrum-averaged $k_\parallel$ presented in the bottom panels of Fig. 5, which show that the amplitude of $\langle k_\parallel \rangle$ for dq/dr (central-averaged) $=2.2$ is significantly higher than for $dq/dr=0.9$, indicating enhanced $k_\parallel$ symmetry breaking with increased radial variation of q. Note the simple relation $k_\parallel = (nq-m)/qR \simeq (n/qR)(dq/dr)(r-r_0)$, near a rational surface at r_0. Given that the turbulence intensity is a reasonable measure of average radial correlation length $\langle (r-r_0) \rangle$, which is at the same level for the three cases of Fig. 5, $\langle k_\parallel \rangle \propto dq/dr$ is readily expected from this simple relation. Therefore, we conclude that the observed enhancement of CTEM-driven intrinsic torque is caused by the enhancement of $k_\parallel$ symmetry breaking with increased radial variation of q.

The key point of this result is that the dependence of the intrinsic torque on dq/dr indeed produces the right trend, which is consistent with the current scaling obtained in Fig. 3. Therefore, given the distinct effects of varying the q value and dq/dr on intrinsic torque generation, it is concluded that the current scaling results from the effect of the nonuniform q profile on the turbulence spectrum. Specifically, the generation of $k_\parallel$ asymmetry in the fluctuation spectrum is enhanced with increased radial variation of q as the current decreases. We should point out that the effect of dq/dr on the nonlinear residual stress generation and the associated key role of it behind the current scaling revealed by these gyrokinetic simulations should be tested and validated by experiments. To a certain extent, this can be done by revisiting the experimental data base from which the current scaling was deduced.

Now we extend our discussion a bit further to examine how CTEM-driven heat transport scales with dq/dr, in comparison with CTEM-driven intrinsic rotation. To this end, we define and calculate a heat transport rate, $d(\Delta Q)/dt$, where $\Delta Q = \int |\Delta T_e| d^3 r$ with ΔT_e the change of electron temperature due to turbulence induced heat transport. Apparently, ΔQ is a measure of electron energy transferred from the high temperature region to the low temperature region, and $d(\Delta Q)/dt$ is the transport rate. The ratio of the momentum generation rate and the heat transport rate is found to increase with the increase of dq/dr, as shown in Fig. 6. The message of this interesting result is quite instructive in terms of the clearly distinct effects of the radial variation of q on rotation generation and energy transport, namely, an increase in dq/dr may enhance the intrinsic rotation generation, but not the heat transport. It also indicates that the underlying dynamics for turbulence driving plasma flow (precisely, the residual stress) and heat transport are quite different. On the other hand, there exists close coupling between turbulence-driven momentum diffusion and thermal diffusion (i.e., $\chi_\phi \sim \chi_i$).[34] Therefore, one may expect quite distinct I_p and dq/dr scalings existing between the diffusive and the nondiffusive momentum transport driven by turbulence. This interesting issue and its implication for experiments will be further discussed in a future publication.

For current scan studies, another scenario often adopted in experiments is to hold the q profile and the pressure profile fixed, while varying the current. In this case, the vacuum magnetic field has to change correspondingly, according to $B_{\rm vac} \propto I_p$. Our nonlinear CTEM simulations have also been carried out to explore the current dependence of intrinsic rotation in this scenario. We used the same simulation parameters as in Fig. 3, except for the MHD equilibria. Simulation results are presented in Fig. 7. In this case, the CTEM-driven intrinsic torque is found to increase with the vacuum field. It is important to notice that in this scan scenario, the parameter ρ_* for the three cases varies significantly, from

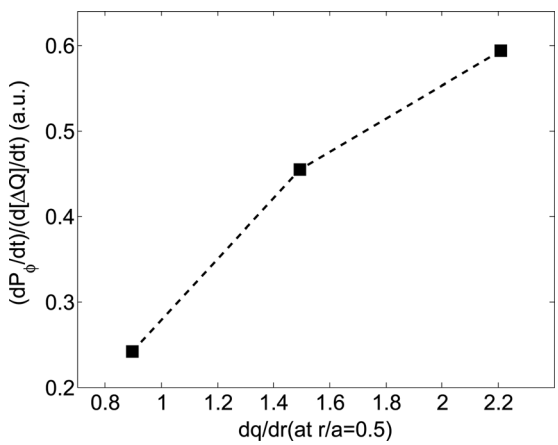

FIG. 6. Ratio of momentum generation rate and heat transport rate vs dq/dr. This is from the same simulations as those of Fig. 5.

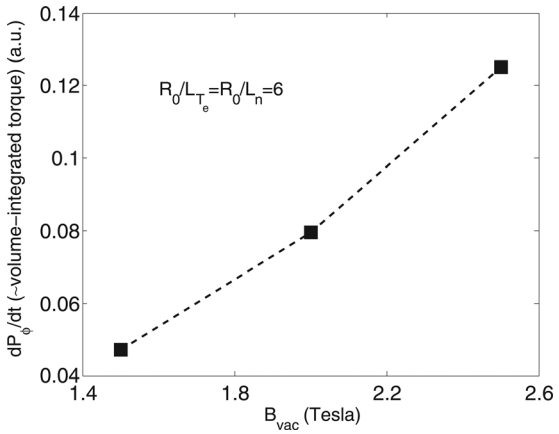

FIG. 7. Total intrinsic torque vs external magnetic field B_{vac} in CTEM turbulence.

$\rho_* \sim 1/130$ for $B_{\text{vac}} = 1.5$ T to $\rho_* \sim 1/230$ for $B_{\text{vac}} = 2.5$ T, which is an important factor impacting turbulence transport. Thus, the variation in ρ_* should be taken into account when we look at the results in Fig. 7 in connection with the experimental scaling. Nevertheless, this current scan scenario is considered to be less relevant to the current scaling obtained in experiments. A possible ρ_*-scaling of turbulence-driven intrinsic torque is a highly important issue in both theory and experiment. However, the B-scan to change I_p performed here may not represent an appropriate way to approach the ρ_*-scaling of intrinsic rotation. To address this issue, more systematic nondimensional scans of various macroscopic parameters are required. The simulation study of the ρ_*-scaling is ongoing research and will be reported elsewhere.

Finally, we should point out that the experimental measurements of intrinsic rotation usually correspond to saturated stationary flow. Like other macroscopic plasma profiles, the stationary flow is developed on the transport time scale which is much longer than that of current gyrokinetic simulations, which are on the turbulence time scale. In the absence of external torque, a steady state of (intrinsic) rotation is reached essentially via the balance between intrinsic torque and momentum dissipation (e.g., due to nonaxisymmetric magnetic perturbation induced viscosity[35]). Therefore, a stationary level of intrinsic rotation depends on how strongly the plasma is driven by intrinsic torque. More specifically, a larger rotation is expected with stronger intrinsic torque. While highly challenging issues remain to be resolved in simulating steady state plasma profiles using gyrokinetic codes, and our simulations presented here do not calculate the steady state intrinsic rotation, the results for the parametric dependence of turbulent torque (i.e., the momentum generation rate) characterized in this section can provide important insight into the behavior and characteristics of steady state intrinsic rotation, thus addressing the physics origin of the empirical scalings.

III. MESOSCALE PHENOMENA IN CTEM TURBULENCE—FLOW, PARTICLE AND HEAT PINCH

A few highly remarkable, interesting features observed in our CTEM simulations are discussed in this section.

Nonlinear GTS simulations have found that mesoscale phenomena and associated nonlocal transport are highly pronounced in the TEM turbulence regime, probably because of strong coherent wave–particle interaction at magnetic precession resonances of trapped electrons. Remarkably, the parallel (and toroidal) flow exhibits coherent temporal burstings and radial propagation during its generation process, as is clearly seen in the upper-left panel of Fig. 8. Particularly, it is shown that small parallel flow perturbations are generated locally (in the center of the plasma in the simulation case) by the turbulence, and then propagate radially. Note that the amplitude of the flow grows with time, as seen in the figure, which is an illustration of intrinsic rotation generation due to the residual stress. The measured propagation velocity is $\sim 7 \times 10^{-3} c_s$, with c_s the sound speed. This "flow pinch" phenomenon observed in the simulations appears to phenomenologically reproduce a well-known experimental result in JT-60U where perturbed flows created by modulated beams were demonstrated to penetrate radially from the peripheral region of the plasma into the core.[7,36] Thus, it is highly illuminating. Furthermore, radial pinches appear to be a very robust and generic feature in CTEM turbulence, and are found to emerge in all transport channels, including particle, electron heat, and ion heat. These are illustrated in Fig. 8. One highly remarkable fact found is that the radial pinches in different transport channels emerge "in phase." We point out that the density pinch and the heat pinch carried by electron turbulence as suggested by our nonlinear CTEM simulations can be tested by designing similar perturbative experiments to the ones with modulated flows.

IV. SUMMARY AND DISCUSSION

Recent progress made with our global gyrokinetic simulations in understanding the origin of intrinsic rotation and plasma flow formation in tokamaks is reported. Critical issues addressed are closely coupled to experimental and theoretical studies with emphasis in this paper on electron transport dominated regimes. The nonlinear flow generation process due to the residual stress produced by the fluctuation intensity and the intensity gradient, in the presence of the low frequency zonal flow shear induced asymmetry in the parallel wavenumber spectrum, is shown to offer one effective, general mechanism to drive intrinsic rotation via wave–particle resonant interaction.

As a most remarkable feature, this turbulence nonlinearly-driven intrinsic rotation is shown to scale close to linearly with plasma gradients and the inverse of the plasma current in various turbulence regimes. Our simulation results not only reproduce the empirical Rice scaling obtained in ion transport dominated experiments, but also extend it into electron transport dominated regimes which are highly relevant to ITER operation. While the turbulence self-generated zonal flow shear provides a key, universal mechanism for $k_{\|}$ symmetry breaking, simulations also indicate that other mechanisms beyond $\mathbf{E} \times \mathbf{B}$ shear enter into play. Such an important mechanism identified in our simulations is the radial variation of the safety factor, which is found to play a critical role in the current scaling. Specifically, the origin of

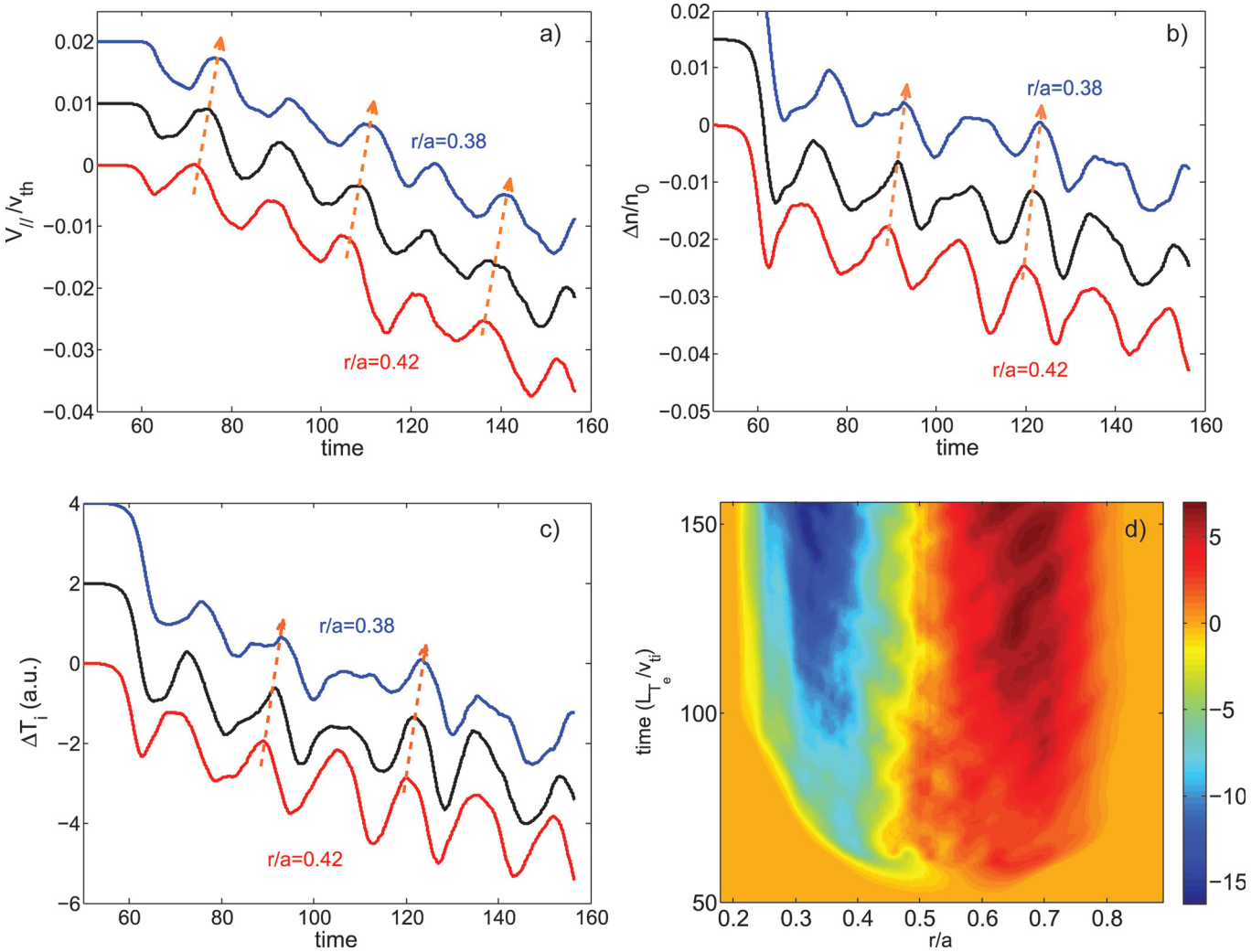

FIG. 8. (Color online) Time history of parallel flow (upper-left), electron density $\Delta n/n_0$ (upper-right), and ion temperature ΔT_i (lower-left) at three radial locations, and spatio-temporal evolution of electron temperature ΔT_e (lower-right) illustrating the generic pinch phenomenon in CTEM turbulence. For illustration purpose, three curves for each quantity of $V_{\|}/v_{\text{th}}$, $\Delta n/n_0$, and ΔT_i at three radial locations are displaced in the direction of the vertical axis. Actually, they all start from zero initially.

current scaling is found to result from the enhancement of $k_{\|}$ symmetry breaking due to increased dq/dr as the current decreases, which enhances the turbulent residual stress and associated intrinsic torque. We point out that this finding from simulations should be confirmed/validated by revisiting the existing experimental data base from which the current scaling was deduced. This kind of validation study is also useful to clarify whether turbulence-driven intrinsic rotation is a major source for the intrinsic rotation observed in experiments. We also want to mention an interesting result that CTEM turbulence-driven transport in different channels, namely momentum, heat, and particles, exhibits qualitatively distinct dependence on plasma current (and the radial variation of q). Specifically, the particle and heat transport do not show considerable dependence on the plasma current and dq/dr. Apparently, our results do not address the well-known, long standing mystery regarding the I_p-dependence of global energy confinement time typically observed in ion thermal transport dominated plasmas, for which the underlying origin might have to do with edge dynamics. On the other hand, the underlying physics governing the intrinsic rotation vs pressure gradient scaling is rather straightforward, namely, both the turbulence intensity and the zonal flow shear, which are two key ingredients for driving residual stress, are increased with the strength of the turbulence drives which are R/L_{T_e} and R/L_{n_e} for CTEM and R/L_{T_i} for ITG. Practically, the scaling of intrinsic rotation $\Delta V_\phi \propto \nabla p$ observed in experiments is strong evidence that turbulence is a key player in driving intrinsic rotation in toroidal devices. Further distinction between $\Delta V_\phi \propto \nabla T_i$ and $\Delta V_\phi \propto \nabla p_e$ may be used to identify which turbulence, ITG or TEM, is dominant, by crosschecks with fluctuation measurements.

Global gyrokinetic simulations have also found that mesoscale phenomena and associated nonlocal transport are largely pronounced in the CTEM turbulence regime due to strong coherent wave–particle interaction at the trapped electron precession frequency. Radial pinches in toroidal flow, heat and particles are robustly driven by CTEM turbulence over a wide range of experimentally relevant parameters. One highlighted feature is that all three pinches emerge "in phase." The pinches can play important roles in determining plasma profiles. Specifically, toroidal flow perturbations,

which are generated locally (in the center of the plasma in the simulation case) by the turbulence, are found to propagate radially. This "flow pinch" result amazingly reproduces the experimental phenomenon of radially inward penetration of perturbed flows created by modulated beams in peripheral regions, and thus is highly illuminating.

A few important open issues which are particularly concerned in simulation studies are briefly discussed. First, while the intrinsic rotation is driven by turbulence nonlinearly generated residual stress, boundary conditions also enter to play roles in determining the formation of the rotation profile. We believe that different boundary conditions should not qualitatively change the key physics captured by the present simulations, e.g., turbulent torque $\propto \nabla p/I_p$. However, they may quantitatively affect the simulated numbers for, e.g., the momentum generation rate, which is certainly important, particularly for comparisons with experiments. Nevertheless, how the intrinsic rotation profile formed depends on various boundary conditions remains to be clarified. For instance, the absorbing boundary condition applied to the inner boundary $(r/a=0.1)$ will be removed by extending the simulation domain to the magnetic axis. This can be achieved by employing artificial cartesian coordinates near the magnetic axis, removing numerical singularities in the region associated with the use of flux coordinates in the present simulations. Further, highly distinct rotation profiles are generated by ITG and by TEM turbulence in simulations with momentum-source-free and initially rotation-free plasmas. Why different rotation profiles are formed between the two turbulence regimes, which are rather robust, remains as a highly interesting issue which is also relevant to experiments. Particle flux, which is driven only in TEM turbulence but not in the adiabatic electron ITG regime, is well known to carry a convective momentum flux, and thus plays roles in reforming the radial profile of turbulence-driven intrinsic rotation in the CTEM regime. The effect of particle flux on the formation of the intrinsic rotation profile, however, remains largely unexplored.

Note that the empirical scalings (Rice scalings) were obtained mostly for H-mode plasmas (some similar scaling was observed in ITB plasmas too). The current GTS simulations do not address edge turbulence in the H-mode pedestal where the equilibrium $\mathbf{E}\times\mathbf{B}$ shear can be large. However, these simulations may have better correspondence to H-mode than to L-mode conditions. In the core region we are simulating, equilibrium $\mathbf{E}\times\mathbf{B}$ shear is subdominant to the turbulence-generated zonal $\mathbf{E}\times\mathbf{B}$ shear. One could, however, expect that for typical H-mode profiles, CTEM turbulence may become more tolerable than ITG turbulence (which usually is the dominant turbulence in L-mode plasmas). We also think that our simple boundary conditions may apply better to H-mode plasmas which exhibit some commonality in rotation behavior, rather than to L-mode plasmas in which rotation shows sensitive dependence on the divertor/limiter configuration.

Experimental evidence shows that the primary intrinsic torque or source of intrinsic rotation appears in the edge/pedestal region, particularly in H-mode plasmas. On the other hand, experiments also observe core intrinsic rotation originating in the core region. To a certain extent, whether a central intrinsic rotation originates locally or from the edge still remains as an open question. It would be relatively straightforward to understand the former case in terms of the turbulence-driven intrinsic rotation revealed in global simulations. If the source of intrinsic torque or intrinsic rotation is in the edge/pedestal region as some experiments suggest,[37] a key question is how central core rotation is coupled with these edge flows/torque? A general argument may include the effects of various momentum pinches[38–41] and possible momentum diffusion. There are some simple models proposed to understand the problem based on these effects.[42] However, a dynamical picture of this process is still missing in a consistent gyrokinetic simulation. Our simulations show that turbulence spreading and the "flow pinch" phenomenon discussed in Sec. III may play a certain role for the edge-core flows/torque coupling. Those results will be presented elsewhere in a future publication. Nevertheless, to fully simulate the dynamics of centrally peaked rotation profile formation represents a highly challenging issue, which may involve flux-driven gyrokinetic simulations on the transport time scale.

ACKNOWLEDGMENTS

The authors would like to express special thanks to Dr. L. Zakharov for generating numerical MHD equilibria using the ESC code for current scan simulations, and Dr. S. Kaye for discussions on how current scan studies are carried out in experiments. We also would like to acknowledge useful discussions with (in alphabetical order) Drs. R. Betti, A. Boozer, L. Chen, G. Dif-Pradalier, J. Q. Dong, X. Garbet, O. Gurcan, C. Hidalgo, F. Hinton, S. Ku, J. Kwon, C. McDevitt, J. Rice, W. Solomon, Y. H. Xu, and H. Zohm. Simulations were performed on Franklin at the National Energy Research Scientific Computing Center (NERSC) and on Jaguar/pf at the National Center for Computational Sciences (NCCS). This work was supported by U.S. DOE Contract No. DE-AC02-09CH11466 and the SciDAC project for Gyrokinetic Particle Simulation of Turbulent Transport in Burning Plasmas.

[1]J. E. Rice, W. D. Lee, E. S. Marmar, P. T. Bonoli, R. S. Granetz, M. J. Greenwald, A. E. Hubard, I. H. Hutchinson, J. H. Irby, Y. Lin, D. Mossessian, J. A. Snipes, S. M. Wolfe, and S. J. Wukitch, Nucl. Fusion **44**, 379 (2004).
[2]Y. Sakamoto, S. Ide, M. Yoshida, Y. Koide, T. Fujita, H. Takenaga, and Y. Kamada, Plasma Phys. Controlled Fusion **48**, A63 (2006).
[3]A. Bortolon, B. P. Duval, A. Pochelon, and A. Scarabosio, Phys. Rev. Lett. **97**, 235003 (2006).
[4]J. S. deGrassie, J. E. Rice, K. H. Burrell, R. J. Groebner, and W. M. Solomon, Phys. Plasmas **14**, 056115 (2007).
[5]L.-G. Eriksson, T. Hellsten, M. F. F. Nave, J. Brzozowski, K. Holmstrom, T. Johnson, J. Ongena, K.-D. Zastrow, and J.-E. Contributors, Plasma Phys. Controlled Fusion **51**, 044008 (2009).
[6]J. E. Rice, A. Ince-Cushman, J. S. deGrassie, L.-G. Eriksson, Y. Sakamoto, A. Scarabosio, A. Bortolon, K. H. Burrell, B. P. Duval, C. Fenzi-Bonizec, M. J. Greenwald, R. J. Groebner, G. T. Hoang, Y. Koide, E. S. Marmar, A. Pochelon, and Y. Podpaly, Nucl. Fusion **47**, 1618 (2007).
[7]M. Yoshida, Y. Kamada, H. Takenaga, Y. Sakamoto, H. Urano, N. Oyama, G. Matsunaga, and the JT-60 Team, Phys. Rev. Lett. **100**, 105002 (2008).
[8]K. Ida, M. Yoshinuma, K. Nagaoka, M. Osakabe, S. Morita, M. Goto, M. Yokoyama, H. Funabe, S. Murakami, K. Ikeda, H. Nakano, K. Ikeda, H. Nakano, K. Tsumori, Y. Takeiri, O. Kaneko, and LHD experiment group, Nucl. Fusion **50**, 064007 (2010).
[9]S. D. Scott, P. H. Diamond, R. J. Fonck, R. J. Goldston, R. B. Howell, K. P. Jaehnig, G. Schilling, E. J. Synakowski, M. C. Zarnstorff, C. E. Bush,

E. Fredrickson, K. W. Hill, A. C. Janos, D. K. Mansfield, D. K. Owens, H. Park, G. Pautasso, A. T. Ramsey, J. Schivell, G. D. Tait, W. M. Tang, and G. Taylor, Phys. Rev. Lett. **64**, 531 (1990).
[10]P. C. de Vries, K. M. Rantamaki, C. Giroud, E. Asp, G. Corrigan, A. Eriksson, M. de Greef, I. Jenkins, H. C. M. Knoops, P. Mantica, H. Nordman, P. Strand, T. Tala, J. Weiland, K.-D. Zastrow, and JET EFDA Contributors, Plasma Phys. Controlled Fusion **48**, 1693 (2006).
[11]S. M. Kaye, W. Solomon, R. E. Bell, B. P. LeBlanc, F. Levinton, J. Menard, G. Rewoldt, S. Sabbagh, W. Wang, and H. Yuh, Nucl. Fusion **49**, 045010 (2009).
[12]P. H. Diamond, C. J. McDevitt, O. D. Gurcan, T. S. Hahm, and V. Naulin, Phys. Plasmas **15**, 012303 (2008).
[13]W. M. Solomon, K. H. Burrell, J. S. deGrassie, R. Budny, R. J. Groebner, J. E. Kinsey, G. J. Kramer, T. C. Luce, M. A. Makowski, D. Mikkelsen, R. Nazikian, C. C. Petty, P. A. Politzer, S. D. Scott, M. A. Van Zeeland, and M. C. Zarnstorff, Plasma Phys. Controlled Fusion **49**, B313 (2007).
[14]W. X. Wang, T. S. Hahm, S. Ethier, G. Rewoldt, W. Lee, W. M. Tang, S. M. Kaye and P. H. Diamond, Phys. Rev. Lett. **102**, 035005 (2009).
[15]W. X. Wang, P. H. Diamond, T. S. Hahm, S. Ethier, G. Rewoldt, and W. M. Tang, Phys. Plasmas **17**, 072511 (2010).
[16]R. Dominguez and G. M. Staebler, Phys. Fluids B **5**, 3876 (1993).
[17]X. Garbet, Y. Sarazin, P. Ghendrih, S. Benkadda, P. Beyer, C. Figarella, and I. Voitsekhovitch, Phys. Plasmas **9**, 3893 (2002).
[18]O. D. Gurcan, P. H. Diamond, T. S. Hahm, and R. Singh, Phys. Plasmas **14**, 042306 (2007).
[19]C. J. McDevitt, P. H. Diamond, O. D. Gurcan, and T. S. Hahm, Phys. Plasmas **16**, 052302 (2009).
[20]F. J. Casson, A. G. Peeters, Y. Camenen, W. A. Hornsby, A. P. Snodin, D. Strintzi, and G. Szepesi1, Phys. Plasmas **16**, 092303 (2009).
[21]Y. Camenen, A. G. Peeters, C. Angioni, F. J. Casson, W. A. Hornsby, A. P. Snodin, and D. Strintzi, Phys. Plasmas **16**, 062501 (2009).
[22]C. J. McDevitt, P. H. Diamond, O. D. Gurcan, and T. S. Hahm, Phys. Plasmas **16**, 012301 (2009).
[23]O. D. Gurcan, P. H. Diamond, P. Hennequin, C. J. McDevitt, X. Garbet, and C. Bourdelle, Phys. Plasmas **17**, 112309 (2010).
[24]A. G. Peeters, C. Angioni, A. Bortolon, Y. Camenen, F. J. Casson, B. Duval, L. Fiederspiel, W. A. Hornsby, N. Kluy, P. Mantica, F. I. Parra, A. P. Snodin, G. Szepesi, D. Strintzi, T. Tala, G. Tardini, P. de Vries, and J. Weiland, in *Proceedings of the 23rd IAEA Fusion Energy Conference, Daejon, Korea* (IAEA Vienna, 2010), IAEA-CN-165/OV/5-4.
[25]J. M. Kwon, S. Ku, S. M. Yi, T. Rhee, S. S. Kim, H. Jhang, L. Terzolo, G. Dif-Pradalier, P. H. Diamond, C. S. Chang, J. Y. Kim, and T. S. Hahm, in *Proceedings of the 23rd IAEA Fusion Energy Conference, Daejon, Korea* (IAEA Vienna, 2010), IAEA-CN-165/THC/3-4Rb.
[26]S. Ku, G. Dif-Pradalier, S. Yi, E. Yoon, P. Diamond, T. Hahm, W. Solomon, C. Chang, Y. Sarazin, V. Grandgirard, J. Abiteboul, X. Garbet, Ph. Gendrih, G. Latu, and A. Strugarek, in *Proceedings of the 23rd IAEA Fusion Energy Conference, Daejon, Korea* (IAEA Vienna, 2010), IAEA-CN-165/PD-2.
[27]W. X. Wang, Z. Lin, W. M. Tang, W. W. Lee, S. Ethier, J. L. V. Lewandowski, G. Rewoldt, T. S. Hahm, and J. Manickam, Phys. Plasmas **13**, 092505 (2006).
[28]J. E. Rice, Z. Yan, M. Xu, G. R. Tynan, P. H. Diamond, O. D. Gurcan, T. S. Hahm, C. Holland, J. Hughes, Y. Kosuga, T. S. Hahm, O. D. Gurcan, R. McDermott, Y. Podpaly, C. J. McDevitt, C. Holland, and S. H. Muller, in *Proceedings of the 23rd IAEA Fusion Energy Conference, Daejon, Korea* (IAEA Vienna, 2010), IAEA-CN-165/EXC/3-3.
[29]Y. Kosuga, P. H. Diamond, and O. D. Gurcan, Phys. Plasmas **17**, 102313 (2010).
[30]B. Scott and J. Smirnov, Phys. Plasmas **17**, 112302 (2010).
[31]A. J. Brizard, private communication (2011).
[32]E. Zakharov and A. Pletzer, Phys. Plasmas **6**, 4693 (1999).
[33]P. H. Diamond, C. J. McDevitt, O. D. Gurcan, T. S. Hahm, W. X. Wang, E. S. Yoon, I. Holod, Z. Lin, V. Naulin, and R. Singh, Nucl. Fusion **49**, 045002 (2009).
[34]N. Mattor and P. H. Diamond, Phys. Fluids **31**, 1180 (1988).
[35]W. Zhu, S. A. Sabbagh, R. E. Bell, J. M. Bialek, M. G. Bell, B. P. LeBlanc, S. M. Kaye, F. M. Levinton, J. E. Menard, K. C. Shaing, A. C. Sontag, and H. Yuh, Phys. Rev. Lett. **96**, 225002 (2006).
[36]M. Yoshida, Y. Koide, H. Takenaga, H. Urano, N. Oyama, K. Kamiya, Y. Sakamoto, K. Kamada, and the JT-60 Team, Plasma Phys. Controlled Fusion **48**, 1673 (2006).
[37]W. M. Solomon, K. H. Burrell, J. S. deGrassie, P. H. Diamond, A. M. Garofalo, T. S. Hahm, C. C. Petty, H. Reimerdes, and R. E. Waltz, in *Proceedings of the 23rd IAEA Fusion Energy Conference, Daejon, Korea* (IAEA Vienna, 2010), IAEA-CN-165/EXC/3-5.
[38]T. S. Hahm, P. H. Diamond, O. D. Gurcan, and G. Rewoldt, Phys. Plasmas **14**, 072302 (2007).
[39]A. G. Peeters, C. Angioni, and D. Strintzi, Phys. Rev. Lett. **98**, 265003 (2007).
[40]J. Weiland, R. Singh, H. Nordman, P. Kaw, A. G. Peeters, and D. Strinzi, Nucl. Fusion **49**, 065033 (2009).
[41]E. S. Yoon and T. S. Hahm, Nucl. Fusion **50**, 064006 (2010).
[42]O. D. Gurcan, P. H. Diamond, C. J. McDevitt, and T. S. Hahm, Phys. Plasmas **17**, 032509 (2010).